AIP | Applied Physics Letters

Kilohertz magnetic field focusing in a pair of metallic periodic-ladder structures

Debasish Banerjee, Jaewook Lee, Ercan M. Dede, and Hideo Iizuka

Citation: Appl. Phys. Lett. **99**, 093501 (2011); doi: 10.1063/1.3629992
View online: http://dx.doi.org/10.1063/1.3629992
View Table of Contents: http://apl.aip.org/resource/1/APPLAB/v99/i9
Published by the AIP Publishing LLC.

Kilohertz magnetic field focusing in a pair of metallic periodic-ladder structures

Debasish Banerjee,[1] Jaewook Lee,[1] Ercan M. Dede,[1] and Hideo Iizuka[1,2,a)]
[1]*Toyota Research Institute, Toyota Motor Engineering & Manufacturing North America, Ann Arbor, Michigan 48105, USA*
[2]*Toyota Central Research & Development Labs., Nagakute, Aichi 480 1192, Japan*

(Received 20 July 2011; accepted 8 August 2011; published online 29 August 2011)

Here, we show, analytically and numerically, that in a pair of metallic periodic-ladder structures placed with a central gap, the normally incident magnetic field is focused on a spot of 3 mm (0.6×10^{-5} free space wavelength) full width at half maximum at a 1 mm distance away at 600 kHz. The ladder structures are designed by exploiting the curl of the induced current at each unit cell in the periodic structure. This investigation paves the way for kilohertz magnetic field manipulations. © *2011 American Institute of Physics*. [doi:10.1063/1.3629992]

Subwavelength focusing of electromagnetic fields is a key technique, used in both optical and microwave regimes, that has been extensively studied to overcome the diffraction limit in a variety of applications. Such applications include superlens,[1] double-slit silver lens,[2] no-hole silver lens,[3] silver-coated Fresnel zone plates,[4,5] aperiodic gold nanowire arrays,[6] subwavelength spaced slot arrays,[7] dielectric gratings,[8] superoscillation,[9] and time-reversal focusing,[10,11] to name a few. Pioneering work on near field focusing schemes based on radiationless interface was presented in Ref. 12, where an appropriately specified field distribution was set on a source to generate a subwavelength focal spot some distance away. The near field plate was designed in Ref. 13 and was experimentally demonstrated in the microwave regime.[14] A corrugated surface structure was also implemented in Ref. 15. In the case of deep subwavelength focusing with substantial energy decay, evanescent fields were amplified by surface polaritons in Ref. 16. The near field focusing scheme was further extended to the optical regime in Refs. 17 and 18 using a nanocircuit concept.[19] No investigation pertaining to the manipulation of kilohertz-band magnetic fields in air has been reported.

In this letter, the focusing scheme based on radiationless interface is extended to magnetic field spatial manipulation in the kilohertz regime. In prior studies for optical and microwave regimes, incident electromagnetic fields were assumed to be parallel to the focusing plates, and the plates were designed by surface impedances (i.e., the ratio of the electric field to the induced current density). Here, a kilohertz band incident magnetic field is assumed to be normal to the focusing plate. The curl of the induced current density at each unit cell is shown to be an important design parameter. Subsequently, a focusing plate is implemented via a pair of metallic periodic-ladder structures.

An analytical model of the focusing plate is shown in Fig. 1(a). This model is composed of fifteen unit cells positioned along the x axis at $z=0$, where the focal plane is located at $z=d$. The incident magnetic field $\vec{H}_{in}(x,z)$ and the transmitted magnetic field $\vec{H}_{trans}(x,z)$ flow along the positive z direction. Zero magnetic field variation is assumed along the y axis. The design procedure starts by formulating the wave equation (1) such that the curl of the induced current density is located on the right hand side of the equation; this represents a point of departure from the mathematical treatment utilized in optical and microwave domains,

$$(\nabla^2 + k^2)\vec{H} = -\nabla \times \vec{J}, \tag{1}$$

where $\vec{H}$ is the magnetic field, $\vec{J}$ is the induced current density, and k is the wave number. The magnetic field is given by integrating the two dimensional Green's function multiplied by the curl of the induced current density,

$$\begin{aligned}\vec{H}(x,z) &= \int G(x,z,x',z'=0)\nabla \times \vec{J}(x')dx' \\ &= -j(1/4)\int Q_0^{(2)}(k((x-x')^2+z^2)^{1/2})\nabla \times \vec{J}(x')dx',\end{aligned} \tag{2}$$

where $Q_0^{(2)}(k((x-x')^2+z^2)^{1/2})$ is the 0th order Hankel function of the 2nd kind. The boundary condition at $z=0$ satisfies the following equation:

$$\begin{aligned}\vec{H}_{trans}(x,z=0) = \vec{H}_{in}(x,z=0) \\ - j(1/4)\int_{-L/2}^{L/2} Q_0^{(2)}(k|x-x'|)\nabla \\ \times \vec{J}(x')dx'.\end{aligned} \tag{3}$$

Once a desired magnetic field distribution $\vec{H}_{trans}(x,z=d)$ is set at the focal plane, the $\vec{H}_{trans}(x,z=0)$ is calculated using back-propagation.[13] Consequently, $\nabla \times \vec{J}(x')$ is obtained. Inversely, in the present case, $\nabla \times \vec{J}(x')$ is fixed in order to fit with eventual simulation results, and the magnetic field $\vec{H}_{trans}(x,z=d)$ is obtained using Eq. (2), with the monochromatic incident field $\vec{H}_{trans}(x,z=0) = H_0 e^{j\omega t}$. Now, the design parameter, $K(x)$, is introduced via the Fredholm integral equation (4) of the second kind, and it may be calculated using the Method of Moments,

a)Author to whom correspondence should be addressed. Electronic mail: hiizuka@mosk.tytlabs.co.jp.

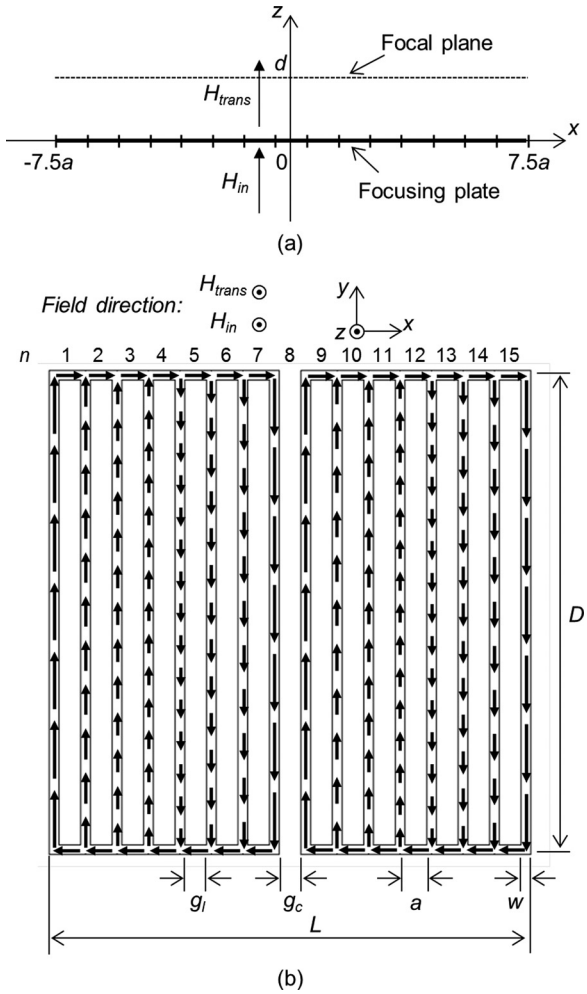

FIG. 1. (a) Analytical model of a focusing plate composed of fifteen unit cells. (b) Focusing plate device implemented via two metallic periodic-ladder structures with a central gap. A snap shot (in time) of the induced current distribution in the device is obtained using COMSOL MULTIPHYSICS. (Dimensions: strip width, $w=0.3$ mm; gap width, $g_c=g_l=1$ mm; unit cell length, $a=w+g_c$ $(g_l)=1.3$ mm; device length, $L=15a+w=19.8$ mm; device height, $D=20$ mm; device thickness, 0.15 mm; focal distance, $d=1$ mm; and conductivity $=5.997\times10^7$ S/m at 600 kHz).

$$\vec{H}_{in}(x)-j(1/4)\int_{-L/2}^{L/2}Q_0^{(2)}(k|x-x'|)\nabla\times\vec{J}(x')dx' = K(x)\nabla\times\vec{J}(x). \quad (4)$$

Specifically, $K(x)$ is the ratio of the magnetic field to the curl of the induced current density at $z=0$ which is a counterpart parameter of the surface impedance found in optical and microwave domains; note that this surface impedance, that is the ratio of the electric field to the induced current density in the case of microwave domains, needs to be imaginary in the design of passive devices. This is seen in the wave equation given by $(\nabla^2+k^2)\vec{E}=j\omega\mu\vec{J}$, where ω and μ are the angular frequency and permeability. While in the kilohertz band, the *K(x)* distribution has real values in the design of such devices as indicated in the relationship of the magnetic field to the curl of the induced current in Eq. (1).

Figure 1(b) shows the configuration of a focusing device. It consists of a pair of metallic periodic-ladder structures positioned with a central gap in the *x*-*y* plane. The

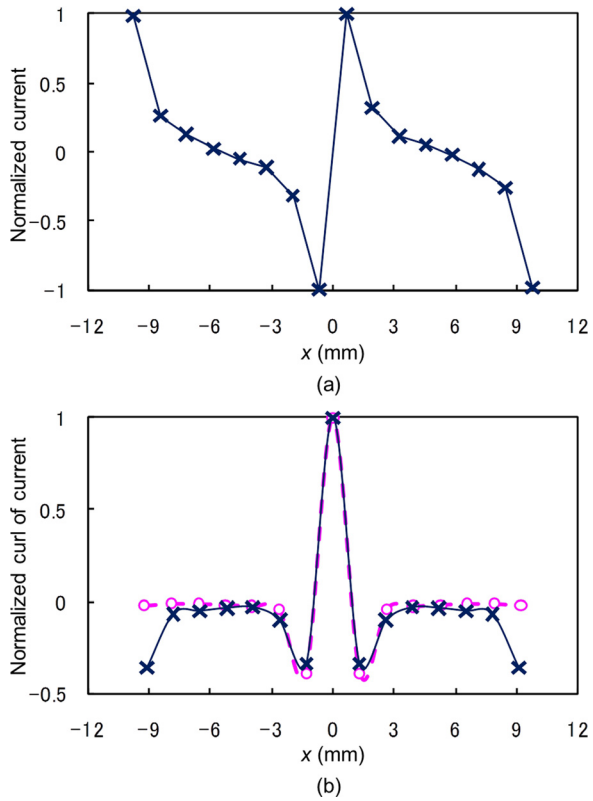

FIG. 2. (Color online) (a) The normalized current (real part) distribution and (b) the curl of the current (real part) distribution at z = 0. The crossed data markers represent the results of the COMSOL MULTIPHYSICS simulation. The circled data markers represent the analytical values that are fitted to the numerical results.

current distribution shown in Fig. 1(b) was obtained with an incident field of 1 A/m in the $+z$ direction using a finite element method based simulation in COMSOL MULTIPHYSICS.[20] Observe that the clockwise currents induced in each ladder structure create a magnetic field, $-\nabla^2\vec{H}=\nabla\times\vec{J}$, that is opposite in direction to that of the incident magnetic field. Also, the current passing through the circumference of the ladder structure exhibits the largest amplitude due to the magnetic flux that passes through the entire structure.

The real part of the simulated current, J_y, in the metallic strips from Fig. 1(b) is plotted in Fig. 2(a), where the plot ranges from $x=-7.5a$ to $+7.5a$ using 16 data points. The current J_y decreases with increasing x except for the crossing at $x=0$ (near the central gap) since clockwise currents are induced in the two ladder structures. Considering only J_y with zero variation assumed along the y direction, $\nabla\times\vec{J}$ is written as $\sim\partial J_y/\partial x$. In this way, the variation of the current, J_y, (crossed markers with solid line) within the unit cell length, a, is plotted over a range from $x=-7a$ to $+7a$ using 15 data points in Fig. 2(b). Note that the $\nabla\times\vec{J}$ distribution has a large peak at the center of the unit cell (i.e., $x=0$) with negative values elsewhere. This large center value in Fig. 2(b) is due to the jump in current at $x=0$ in Fig. 2(a). Furthermore, the remaining off center negative values evident in Fig. 2(b) are an artifact of the current decreasing as a function of x in Fig. 2(a). Additionally, the analytical $\nabla\times\vec{J}$ distribution (circled markers with dashed line) is fitted to the simulation data (crossed markers with solid line), as shown in Fig. 2(b). The imaginary parts of the current and magnetic

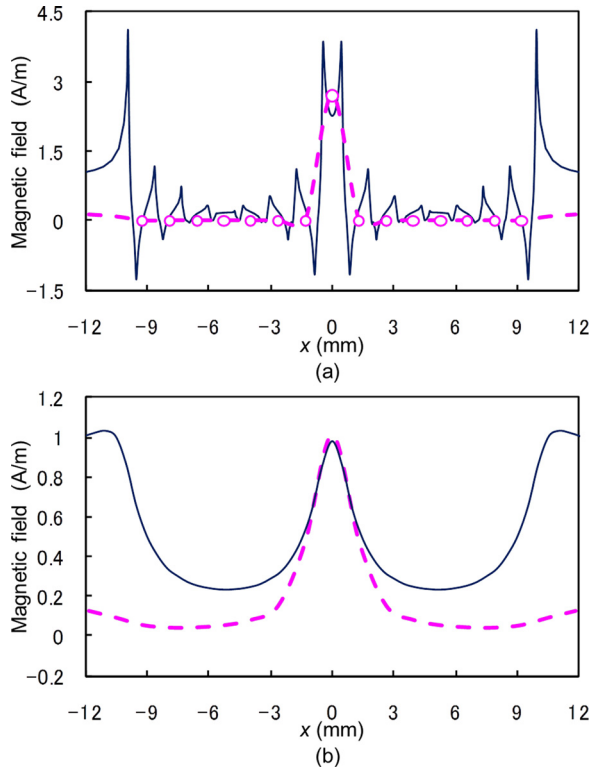

FIG. 3. (Color online) (a) Magnetic field (real part) distributions at (a) $z=0$ and (b) $z=1$ mm. The dashed lines are obtained using the analytical model, Fig. 1(a), and the circled markers represent fifteen sampling points at $z=0$. The solid lines represent the results of the COMSOL MULTIPHYSICS simulation, Fig. 1(b).

fields are relatively small in comparison with the real parts, i.e., $\mathrm{Im}(J_y)/\mathrm{Re}(J_y)<0.1$ in Fig. 2(a), and are not presented here due to space constraints.

Figures 3(a) and 3(b) show the real part of the magnetic field intensity distributions at $z=0$ and 1 mm, respectively. The analytical magnetic field distribution at $z=0$ (circled markers with dashed line) is obtained by incorporating the $\nabla\times\vec{J}$ distribution of Fig. 2(b) into Eq. (3), where each circled marker is located at the center of each unit cell, i.e., $x=(n\text{-}8)a$ for $n=1$ to 15. The field distribution has a central peak of 2.7 A/m due to a scaling factor of 2.7 that compensates for the field decay in the z direction. Using Eq. (2), a magnetic field with a 2.8 mm full width at half maximum (FWHM) at $z=1$ mm (dashed line) is calculated. Observe that the simulated magnetic field at $z=0$ (solid line) also exhibits a central peak. Field fluctuations are evident near the metallic strips at $x\sim(2m\text{-}17)a/2\pm w/2$ for $m=1$ to 16. These fluctuations are due to a sharp turn in the current at the rungs of the periodic ladder structure which causes noticeable variations in the magnetic field lines, per the basic relation $\nabla\times\vec{H}=\vec{J}$. Regardless, the numerical and analytical results are in reasonable agreement for the $z=0$ magnetic field distribution at each sampling point. It is also worth noting that the central simulated magnetic field at $z=0$ is 2.3 times larger than the input magnetic field of 1 A/m. This enhancement is due to the variation of the different directional large currents within a one-unit cell length, where the large currents are induced by the magnetic flux for the entire ladder structure. This spatial redistribution of the magnetic field via the ladder structures can be envisioned to produce magnetic field focusing. The focusing device from Fig. 1(b) has a spot of 3 mm FWHM at $z=1$ mm (solid line), as shown in Fig. 3(b). It must be emphasized that the magnetic field may indeed be focused on a spot of $0.6\times10^{-5}\ \lambda_0$ FWHM by the focusing device having a device length of $\sim4\times10^{-5}\ \lambda_0$, where λ_0 is a free space wavelength of 500 m. A discrepancy is seen in the skirt curves of the $z=1$ mm magnetic field. The simulated magnetic field decreases from $x=0$ to $|x|\sim5$ mm, and then increases to the amplitude of the incidence, 1 A/m, $|x|>10.5$ mm (outside of the device). This behavior is mainly due to the fact that the incident magnetic field is applied not only to the device area but also to the area outside of the device. In contrast, the analytical result displays only a central peak since the incident magnetic field is applied exclusively to the device area. For reference, when the device is doubled in length with 30 unit cells, $30a+w=39.3$ mm in the x direction, the minimum level in the magnetic field at $z=1$ mm decreases from 0.23 A/m at $|x|\sim5$ mm to 0.17 A/m at $|x|\sim10$ mm.

From an energy flow perspective, both the Poynting vector, $\vec{E}\times\vec{H}^*$, and electric energy density, $(1/2)\varepsilon_0\vec{E}\cdot\vec{E}^*$, are significantly smaller in magnitude than the magnetic energy density, $(1/2)\mu_0\vec{H}\cdot\vec{H}^*$. This is due to the kHz range device under consideration having $|\vec{E}|$ much less than $|\vec{H}|$ at the focal plane. As a result, the ratio of the electric to magnetic energy densities is found numerically to be $\sim10^{-7}$. Consequently, the energy flow at the focal plane is characterized primarily by the magnetic energy density, $\sim(1/2)\mu_0|\vec{H}_{trans}(x,z=1\ mm)|^2$.

In conclusion, a concept of kilohertz magnetic field focusing was theoretically proposed, and a spot of 3 mm FWHM was numerically demonstrated in a double periodic-ladder structure. This investigation paves the way for kilohertz magnetic field manipulations.

We acknowledge fruitful discussions with Dr. Mindy Zhang, Dr. Michael Rowe, and Dr. Joy Wu.

[1]J. B. Pendry, Phys. Rev. Lett. **85**, 3966 (2000).
[2]K. R. Chen, Opt. Lett. **35**, 3763 (2010).
[3]P. Wrobel, J. Pniewski, T. J. Antosiewicz, and T. Szoplik, Phys. Rev. Lett. **102**, 183902 (2009).
[4]Y. Fu, W. Zhou, and L. E. N. Lim, Appl. Phys. Lett. **91**, 061124 (2007).
[5]R. G. Mote, S. F. Yu, B. K. Ng, W. Zhou, and S. P. Lau, Opt. Express **16**, 9554 (2008).
[6]L. Verslegers, P. B. Catrysse, Z. Yu, and S. Fan, Phys. Rev. Lett. **103**, 033902 (2009).
[7]L. Markley, A. M. H. Wong, Y. Wang, and G. V. Eleftheriades, Phys. Rev. Lett. **101**, 113901 (2008).
[8]A. Sentenac and P. C. Chaumet, Phys. Rev. Lett. **101**, 013901 (2008).
[9]F. M. Huang and N. I. Zheludev, Nano Lett. **9**, 1249 (2009).
[10]G. Lerosey, J. de Rosny, A. Tourin, and M. Fink, Science **315**, 1120 (2007).
[11]E. Mudry, E. LeMoal, P. Ferrand, P. C. Chaumet, and A. Sentenac, Phys. Rev. Lett. **105**, 203903 (2010).
[12]R. Merlin, Science **317**, 927 (2007).
[13]A. Grbic, and R. Merlin, IEEE Trans. Antennas Propag. **56**, 3159 (2008).
[14]A. Grbic, L. Jiang, and R. Merlin, Science **320**, 511 (2008).
[15]M. F. Imani, and A. Grbic, IEEE Antennas Wireless Propag. Lett. **8**, 421 (2009).
[16]V. Intaraprasonk, Z. Yu, and S. Fan, Opt. Lett. **35**, 1659 (2010).
[17]R. Gordon, Phys. Rev. Lett. **102**, 207402 (2009).
[18]L. Scorrano, F. Bilotti, and L. Vegni, Microw. Opt. Tech. Lett. **51**, 2718 (2009).
[19]N. Engheta, Science **317**, 1698 (2007).
[20]COMSOL MULTIPHYSICS, ver.4.1, http://www.comsol.com.